Ex vivo aortic stiffness in mice with different eNOS activity

Ex vivo aortic stiffness in mice with different eNOS activity.

Arthur J.A. Leloup[1], Cor E. Van Hove[2], Sofie De Moudt[1], Gilles W. De Keulenaer[1, 3], Paul Fransen[1]

[1] University of Antwerp, Department of Pharmaceutical Sciences, Laboratory of Physiopharmacology, Campus Drie Eiken, Universiteitsplein 1, B-2610 Antwerp, Belgium

[2] University of Antwerp, Faculty of Medicine and Health Sciences, Laboratory of Pharmacology, Campus Drie Eiken, Universiteitsplein 1, B-2610 Antwerp, Belgium

[3] Department of Cardiology, Middelheim Hospital, Lindendreef 1, 2020 Antwerp, Belgium

Correspondence:

Paul Fransen

Department of Pharmaceutical Sciences

Campus Drie Eiken - D.T.228

Universiteitsplein 1 - 2610 Wilrijk - Belgium

Paul.fransen@uantwerpen.be

Running head: eNOS expression and aortic stiffness

Word count: 8031

Abstract

An important physiological role of the aorta is to convert the pulsatile blood flow that originates in the heart to a nearly-continuous flow in the peripheral vessels. Previously, we demonstrated that basal, unstimulated NO production is more abundant in large as compared to muscular arteries and that it is an important regulator of arterial (aortic) stiffness. Hence, endothelial function and NO bioavailability are important determinants of aortic biomechanics and mouse models with altered NO signaling might be of interest to investigate the (patho)physiological role of the NO signaling as a dynamic regulator of arterial stiffness. We aimed to characterize the ex vivo biomechanical properties of aortic segments from mice with no ($eNOS^{-/-}$), normal (WT) or high (eNOS-tg) endothelial NO synthase (eNOS) expression. Isobaric aortic diameter and compliance were lower in $eNOS^{-/-}$ mice and increased in eNOS-tg mice as compared to WT mice. Interestingly, these differences remained when NO levels were pharmacologically restored ex-vivo, suggesting that they were not merely the result of a lack or excess of the vasodilator effects of NO. Analysis of basal vascular smooth muscle cell tone and the phasic as well as the tonic contraction in response to α_1-adrenergic stimulation with phenylephrine revealed that the chronic lack of eNOS expression affected aortic reactivity similarly but with different magnitude as compared to acute eNOS blockade using L-NAME in WT and eNOS-tg mice, suggesting that chronical distortion of NO signaling triggered several compensatory mechanisms that reflect the organism's attempt to restore the contractile imbalance and maintain optimal central hemodynamics.

New and noteworthy Endothelial function and NO bioavailability are important determinants of aortic biomechanics and function. With a new technique we investigated the ex-vivo aortic segment biomechanics of different mouse models with altered NO signaling. Our experiments clearly show that chronic distortion of NO signaling triggered several compensatory mechanisms that reflect the organism's attempt to maintain optimal central hemodynamics.

Key words: aortic stiffness, mouse, eNOS, endothelium, vascular smooth muscle cell

1. Introduction

Progressive large artery stiffening is the predominant cause of increased pulse pressure, a marker of cardiovascular (CV) risk in the general population (4) and a predictor of CV events (34) . Furthermore, it reduces myocardial perfusion efficiency, increases left ventricular afterload and elicits mechanical stress on capillaries, potentially damaging the capillary wall of strongly perfused organs such as the heart, brain and kidneys (42). In the recent years, arterial stiffness was shown to precede hypertension during vascular aging both in humans (21, 36) and in animal models (52), rendering it a promising therapeutic target to treat CV disease.

About one third of the large artery wall volume consists of vascular smooth muscle cells (1, 10) that contract and relax in response to neurogenic, mechanical, humoral and local stimuli, thereby altering the biomechanical properties of the large arterial wall (3, 25, 30, 34, 40, 54). In addition to VSMCs, endothelial cells are important mediators of arterial tone, mostly via acting on VSMCs. An important mediator of VSMC tone is the endothelium-derived relaxing factor nitric oxide (NO). NO is produced by the endothelial NO synthase (eNOS) and diffuses to the VSMCs where it activates the NO-sensitive guanylate cyclase, leading to cyclic guanosine monophosphate (cGMP)-mediated relaxation. The expression and activity of eNOS and its downstream targets are tightly regulated (2, 23, 40, 46) and endothelial dysfunction is associated with aging and large artery stiffening (19, 49). The link between NO and arterial compliance has been demonstrated both *ex vivo* (30, 39) and *in vivo* (22, 47). We recently showed that elastic arteries produce large amounts of NO in basal, non-stimulated conditions, while muscular arteries do not (29). Since elastic arteries, in contrast to muscular arteries, are prone to stiffening (5, 42, 55). Basal NO deficiency was also observed very early in the disease progression in isolated arteries of several mouse models with arterial disease (24, 32). Moreover, we recently investigated how the pharmacodynamic properties of isolated aortic segments of healthy mice determine the VSMC contraction-associated changes in aortic stiffness. Interestingly, basal NO production protected the aorta from the stiffening-effects of phenylephrine (PE) ex vivo, at concentrations equivalent to the circulating catecholamine levels *in vivo* (31), further supporting our

hypothesis that basal NO metabolism is a crucial (patho)physiological regulator of large artery stiffness.

Mouse models with different expression levels of eNOS are available and well-characterized. Compared to WT mice, $eNOS^{-/-}$ mice display increased blood pressure (17, 52), pulse wave velocity (28, 48) and increased isobaric stiffness (20). Some studies report a reduced heart rate (48), others show no heart rate-effect (20). As expected, no endothelium-dependent relaxation is seen on isolated aortic segments (17). In addition, $eNOS^{-/-}$ are reported to have lower body weight and altered blood glucose, cholesterol, insulin and leptin levels (42), renal dysfunction (51), neurochemical and behavioral adaptations (8, 9), cardiac abnormalities (14, 26, 51), reduced ovulatory efficiency and oocyte maturation (18) and altered platelet aggregation (13). The overexpression of eNOS in mice is shown to result in lower blood pressure and heart rate (15). Studies reporting a role of eNOS overexpression on cholesterol levels (15, 44) and protection against liver damage after ischemia/reperfusion injury (11, 39) are conflicting. Body weight was shown to be decreased in eNOS overexpressing mice and metabolic activity in adipose tissue is shown to be affected (44). To our knowledge, the effects of eNOS overexpression on large artery reactivity and biomechanics are unknown.

Given the role of eNOS expression and activity on large artery EC and VSMC function as well as the contribution of VSMC tone to aortic wall stiffness (30), we hypothesized that altered expression levels of eNOS affect the biomechanical properties of the aorta through changes in VSMC tone. Therefore we aimed to characterize the morphology and function of aortic segments from eNOS knock-out mice and from mice overexpressing eNOS. An in-house developed set-up was used to analyze isobaric stiffness parameters, both in passive, unstimulated, and in active conditions. We performed histological staining on aortic slides to assess general structure and morphology of the aortic wall. Lastly, isometric contraction studies on aortic segments were performed to assess VSMC and EC reactivity.

2. Materials and methods

2.1. Animals and tissue preparation

All studies were approved by the Ethical Committee of the University of Antwerp, and the investigations conform to the Guide for the Care and Use of Laboratory Animals published by the US National Institutes of Health (NIH Publication no.85-23, revised 1996). All animals (C57Bl/6J background, male, +/- 5 months old) were bred and housed in the animal facility of the University of Antwerp in standard cages with 12h-12h light-dark cycles with free access to regular chow and tap water. The following mice were used: male C57Bl/6J (WT) mice (n=6), male $eNOS^{-/-}$ mice (n=5) on C57Bl/6J background and male C57Bl/6J mice with a knock-in of a human eNOS construct, fused with a GFP tag (eNOS-tg (n=6), a kind gift of R. Van Haperen). As described before, eNOS activity in aortic tissue was increased ~35-fold and NO bioavailability approximately doubled (15). Animals were euthanized by perforating the diaphragm while under deep anesthesia (sodium pentobarbital (Sanofi, Belgium), 75 mg kg-1, i.p.). The thoracic aorta was carefully removed and stripped of adherent tissue. Starting at the diaphragm, the aorta was cut in 5 segments of 2 mm width. One segment was mounted in an oscillating organ bath to study the biomechanical properties (see further), the others in standard organ baths to study the isometric contraction. The segments were immersed in Krebs-Ringer (KR) solution (37°C, 95% O_2/5% CO_2, pH 7.4) containing (in mM): NaCl 118, KCl 4.7, $CaCl_2$ 2.5, KH_2PO_4 1.2, $MgSO_4$ 1.2, $NaHCO_3$ 25, CaEDTA 0.025 and glucose 11.1. To avoid any vasomotor interference due to prostanoids, 10 μM indomethacin (Federa, Belgium) was present in all experiments.

2.2. Oscillating organ bath

In order to assess isobaric diameter contraction or relaxation and isobaric parameters of aortic stiffness, a 5 ml organ bath that allowed periodic clamping of the aortic segment at given preloads or diameters, was used. This system is similar to a traditional organ bath but with a horizontal force-length transducer described earlier (6, 7). In short, one hook was fixed, the other one connected to a lever from the force-length transducer. This lever was connected to a coil suspended in a strong field

of a permanent magnet. The system was controlled by a current source. When current was passed through this coil, a force was developed. The displacement of the lever was measured by means of a photo-electric system. The transducer was connected to a data acquisition system (Powerlab 8/30 and LabChart 7, ADInstruments). Force and displacement were acquired at 1 kHz.

The lever displacement was recalibrated to vessel diameter via the internal circumference of the aortic segment, as determined using a calibrated stereomicroscope. The length of the segment (~2 mm as described earlier) was determined at least 4 times during the protocol and averaged in order to estimate transmural pressure using Laplace's law

$$P = \frac{F}{l.D}$$

with F being the force as measured by the transducer, D and l the diameter and length of the vessel segment, respectively. This allowed us to adjust the diastolic and systolic preload until calculated transmural pressures of 80-120 mmHg were achieved. Compliance (µm/mmHg) was determined as follows:

$$C = \frac{\Delta D}{\Delta P}$$

with ΔD and ΔP (~40 mmHg) being the diameter and pressure difference, respectively. Peterson's pressure-strain modulus, a frequently used parameter of arterial stiffness was determined as follows:

$$Ep = D_0.\frac{\Delta P}{\Delta D}$$

with D_0 the diastolic diameter.

During all experiments, segments were stretched between 80 mmHg and 120 mmHg at a frequency of 10 Hz (600 bpm). Diastolic diameter contraction or relaxation, compliance and Ep were determined for aortic segments from all three genotypes in the presence of 2 µM PE and in the presence of 2 µM DEANO, as compared to KR solution, to assess the maximal active and passive (i.e. in the absence of

VSMC tone) stiffness, respectively. In all cases, stretch amplitude was kept constant at 40 mmHg (10 Hz).

2.3. Histology

Segments were fixed with 4 % paraformaldehyde for 24h, dehydrated overnight in 60% isopropanol and embedded in paraffin. Histological analysis was performed on serial cross sections (5µm) stained with hematoxylin and eosin, orcein, and sirius red stain to visualize general morphology, elastin and collagen, respectively. The images were acquired with the Universal Grab 6.1. (IDL) software (Exelis, Boulder, CO) using an Olympus BX40 microscope (Tokyo, Japan). ImageJ was used to analyze circumference, wall thickness (20-40 measurements, averaged), elastin or collagen content (elastin or collage-positive pixels relative to the total amount of wall pixels) and VSMC content.

2.4. Isometric contraction studies

Aortic segments were mounted in 10 ml organ baths as previously described (16) at a preload of 30 mN. Isometric contraction force is reported in mN. To inhibit basal NO formation by the endothelium, 300 µM N^{Ω}-nitro-L-arginine methyl ester (L-NAME) was added. To deplete all Ca^{2+} from the KR solution and to measure phasic contractions by PE in the absence of external Ca^{2+}, nominal Ca^{2+} free KR was supplemented with 1 mM EGTA (further named 0Ca). After addition of 2 µM of the α1-adrenergic agonist PE, the amplitudes (A_{on}) and time constant (τ_{on}) of the phasic contraction as well as the amplitudes (A_{off}) and time constants (τ_{off}) of the subsequent relaxation were studied by performing a bi-exponential analysis of these contractions

$$Y = A_{on}\left[1 - e^{-K_{on}(t-t_0)}\right] + A_{off}\left[1 - e^{-K_{off}(t-t_0)}\right]$$

with Y being force (mN), A_{on} being the amplitude of the contractile phase, K_{on} being the rate constant of contraction ($1/\tau_{on}$), t being the time (s), t_0 being the start time of contraction (± 10 ms), A_{off} being the amplitude of relaxation and K_{off} being the rate constant of relaxation ($1/\tau_{off}$).

To restore normal external Ca^{2+} to 2.5 mM and elicit a tonic contraction, 3.5 mM Ca^{2+} was added to the 0Ca KR. Subsequently, the tonic contraction was (partly) inhibited using either the voltage gated calcium channel (VGCC) blocker diltiazem (30 μM) or 2-minoethoxydiphenyl borate (2-APB, 50 μM).

2.5. Statistics

All results are expressed as mean±SD; n represents the number of mice. Parametric one-way or two-way ANOVA or non-parametric Kruskal-Wallis tests were used. When multiple pairwise comparisons were performed, p-values were adjusted using Bonferroni or Dunn's methods, as specified in the figure legends. All analyses were performed using GraphPad Prism (version 5, GraphPad Software, San Diego California USA). A 5% level of significance was selected.

2.6. Materials

Sodium pentobarbital (Nembutal®) was obtained from Sanofi (Brussels, Belgium), indomethacin from Federa (Belgium), L-NAME, phenylephrine hydrochloride (PE) and diethylamine NONOate (DEANO) from Sigma-Aldrich (Bornem, Belgium), diltiazem hydrochloride from TOCRIS (Bristol, United Kingdom).

3. Results

3.1. Isobaric measurement of passive and active wall biomechanics

Isobaric dimensional and biomechanical parameters were measured to assess the intrinsic properties of the aortic wall. Diameter of thoracic aorta segments at simulated diastolic pressure of 80 mm Hg was significantly smaller ($P<0.05$) in $eNOS^{-/-}$ mice and significantly increased ($P<0.05$) in eNOS-tg mice (figure 1A). Similar observations were made for isobaric compliance, which was significantly higher ($P<0.05$) in eNOS-tg and lower ($P<0.05$) in $eNOS^{-/-}$ aortic segments (figure 1B). Ep was significantly elevated ($P<0.05$) in $eNOS^{-/-}$ vs WT aortic segments (figure 1C). Ep of aortic segments of eNOS-tg mice, however, was not significantly different ($P>0.05$) from Ep of WT aortic segments, indicating

that morphological but not intrinsic mechanical properties of the aortic wall are responsible for the increased compliance in the eNOS-tg aortic segments.

To investigate whether exogenous NO could eliminate the differences between the three strains, 2 μM DEANO was added to maximally relax VSMCs and to remove any baseline tonus. The passive, isobaric diameter, compliance and stiffness (figure 2A-C) were similar to baseline conditions in KR solution ($P>0.05$). The magnitude of the effects of DEANO (vs. baseline (KR)) was not significantly different between groups (figure 2A-C, $P>0.05$), i.e. exogenous NO could not reverse the reduced diameter or compliance or increased stiffness in $eNOS^{-/-}$ segments.

To measure the maximal amount of stiffness development due to VSMC contraction, 2 μM PE was added to the organ bath (figure 3). This resulted in isobaric diameter constriction ($P<0.05$), decreased ($P<0.05$) isobaric compliance and increased ($P<0.05$) Ep (figures 3A-C). However, the differences between the groups as observed in KR or KR + DEANO remained. While $eNOS^{-/-}$ aortic segments had smaller diameter, lower isobaric compliance and higher isobaric Ep, the aortic segments from eNOS-tg mice had significantly larger diastolic diameter ($P<0.05$) and compliance ($P<0.05$) but Ep was not significantly different ($P>0.05$) from WT aortic segments. The effects of PE on diameter, compliance and Ep are displayed in figure 3D, E and F. When 2 μM PE was added to the organ bath, $eNOS^{-/-}$ aortic segments constricted significantly more ($P<0.05$) than WT aortic segments (figure 3D). As expected, compliance decreased more ($P<0.05$) in $eNOS^{-/-}$ aortic segments (figure 3E). Ep increased significantly more ($P<0.05$) in $eNOS^{-/-}$ aortic segments as compared to WT aortic segments (figure 3F). The effects of PE on isobaric diameter, compliance and Ep were not significantly different ($P>0.05$) between WT and eNOS-tg mice, indicating that the functional efficacy of NO (i.e. suppressing the contractile or stiffening effect of PE in baseline conditions) was similar in WT and eNOS-tg mice.

3.2. Morphology

Aortic segments of WT, $eNOS^{-/-}$ and eNOS-tg mice were stained with hematoxylin-eosin (H&E) for general morphology, with orcein to visualize elastin and with sirius red to stain collagen (figure 4).

The staining allowed to express different wall structure parameters as shown in figure 5. Internal circumference (figure 5A) and wall thickness (figure 5B) are larger ($P<0.05$) in eNOS-tg mice than in control or $eNOS^{-/-}$ mice. The aortic wall surface area (figure 5C) is significantly larger ($P<0.05$) in eNOS-tg and smaller ($P<0.05$) in $eNOS^{-/-}$ mice than in WT mice. These data confirm the differences in isobaric aortic diameter observed in the previous experiments. The number of VSMCs per wall surface area is significantly decreased ($P<0.05$) in $eNOS^{-/-}$ and eNOS-tg mice. The amount of elastin is not significantly different ($P>0.05$) between $eNOS^{-/-}$ and WT mice but slightly decreased in eNOS-tg mice, whereas no significant differences ($P>0.05$) were demonstrated for the collagen content of the aortic wall.

3.3. Isometric properties of the aortic wall.

Arterial stiffness increase in $eNOS^{-/-}$ aortic segments could not be compensated for by adding exogenous NO (figure 2) and also morphological characteristics could not explain the increased stiffness ($P>0.05$). In isometric experiments we investigated whether basal Ca^{2+} influx contributed to basal VSMC tone. When extracellular Ca^{2+} was removed from the KR solution, a small, but significant ($P<0.05$) decrease of preload was induced in $eNOS^{-/-}$ aortic segments (figure 6A). When the experiments were repeated but now in the presence of L-NAME to block basal NO release, there was – as expected – no further significant change of the preload in the $eNOS^{-/-}$ aortic segments. However, in WT and eNOS-tg mice the inhibition of basal NO release with L-NAME caused a significant baseline influx ($P<0.05$) of extracellular Ca^{2+}, which was significantly larger than in $eNOS^{-/-}$ aortic segments (figure 6B).

Subsequent α_1-adrenoceptor stimulation of the aortic segments with 1 μM PE in the absence of extracellular Ca^{2+} caused phasic contractions as shown in figure 7A and B. These contractions significantly differed ($P<0.05$) between WT and $eNOS^{-/-}$ and eNOS-tg mice before and after inhibition of basal NO release with 300 μM L-NAME, as shown in figure 7C to F. An exponential analysis of these contractions revealed that the contraction amplitude was significantly larger ($P<0.05$) in $eNOS^{-/-}$ and eNOS-tg mice in the absence of L-NAME. L-NAME increased contraction amplitude in WT

239 ($P<0.05$) and eNOS-tg mice wiping out the differences between the amplitudes as observed in the
240 absence of L-NAME. The time constant of contraction (τ_{on}) was larger in $eNOS^{-/-}$ mice than in WT or
241 eNOS-tg mice only in the absence of L-NAME ($P<0.05$). The time constants of relaxation (τ_{off}) were
242 significantly smaller ($P<0.05$) in $eNOS^{-/-}$ mice and larger in eNOS-tg mice ($P<0.05$) independent of
243 the activity of eNOS.

244 Addition of external Ca^{2+} after the phasic contraction caused a tonic contraction (figure 8), which was,
245 in the absence of L-NAME, significantly larger ($P<0.05$) in $eNOS^{-/-}$ and eNOS-tg aortic segments than
246 in WT segments. In the presence of L-NAME, the contraction by PE increased significantly in WT
247 and eNOS-tg mice ($P<0.05$), but did not change in $eNOS^{-/-}$ mice ($P>0.05$). When the contraction in the
248 absence of L-NAME was expressed as a function of the contraction in the presence of L-NAME, it is
249 evident that in the absence of eNOS inhibition, the contraction of WT and eNOS-tg aortic segments
250 was about 40 to 60% suppressed by basal NO release, whereas $eNOS^{-/-}$ segments did not produce basal
251 NO (figure 8D).

252 After 10 minutes the tonic contraction by PE was inhibited by addition of 35 μM diltiazem to reveal
253 the contribution of VGCC Ca^{2+} influx to the contraction. Subsequently the contraction was further
254 inhibited with 50 μM 2-APB, which, at this concentration, mainly blocks contractile Ca^{2+} influx via
255 non-selective cation channels (NSCCs). As such, it is possible to reveal the relative contribution of
256 VGCC and NSCC Ca^{2+} influx to the contraction of aortic segments by PE in the three different strains
257 (figure 9).

258 The tonic contraction by PE (figure 9C) is mainly due to Ca^{2+} influx via VGCCs (figure 9A and C). In
259 general 80% of the PE-induced tonic contraction is inhibited by 35 μM diltiazem in WT and eNOS-tg
260 aortic segments, whereas the inhibition is significantly attenuated in $eNOS^{-/-}$ segments ($P<0.05$).
261 Normally, basal NO inhibits the influx of Ca^{2+} through NSCCs. In the presence of L-NAME, Ca^{2+}
262 influx via NSCCs is activated, especially in WT and eNOS-tg mice, whereas in $eNOS^{-/-}$ mice the
263 contribution of NSCC Ca^{2+} influx to the contraction is even decreased (figure 9B and D, $P<0.05$). The

contribution of VGCC Ca^{2+} influx to the contraction in these mice is in absolute and relative value larger ($P<0.05$) in $eNOS^{-/-}$ than in WT or eNOS-tg segments.

4. Discussion

In the present study, aortic segments from two mouse models of differential eNOS expression were compared with aortic segments from WT mice. We focused on intrinsic passive (structural) and active aortic wall biomechanical properties using an in-house developed oscillating organ bath, on general structural and morphological differences using histological staining, and on vascular reactivity by means of isometric contraction studies. An overview of the main conclusions is given in table 1. Ep, a parameter of arterial stiffness, was significantly higher in $eNOS^{-/-}$ mice. eNOS-tg and WT mice did not differ significantly, indicating that the morphological (i.e. increased aortic diameter) but not the intrinsic wall properties of the eNOS-tg aortic rings are responsible for the observed differences in compliance. Caution is required when linking the morphological parameters derived from histological staining to the biomechanical parameters that reflect the complex interplay between extracellular matrix composition and organization and active contribution of VSMC and EC cross-talk. Indeed, a large part of the active, contractile and biomechanical properties are affected by the VSMCs. Differences in the cytoskeletal properties or even the absolute numbers of VSMCs might thus affect vessel contractility and biomechanics. Unloaded diameter, wall thickness and surface were increased in eNOS-tg aortic segments as shown in histological staining. In KR solution, isobaric diameter at 80 mmHg confirmed the histological (unloaded) diameters, i.e. $eNOS^{-/-}$ and eNOS-tg aortic segments have a smaller and larger diameter as compared to WT aortic segments, respectively. However, in eNOS-tg aorta, orcein staining indicated lower amount of elastin per unit of surface area, while compliance of the segments was increased. $eNOS^{-/-}$ aortic segments were less compliant, while no significant differences in elastin or collagen content.

To determine the isobaric biomechanical properties in the absence of basal Ca^{2+} influx, excess exogenous NO (2 μM DEANO) was added to the organ bath. The effects of DEANO were very small and of similar magnitude in all three groups. This indicates that the stiffness seen in the $eNOS^{-/-}$ aortic

rings in KR solution are not a direct result of the lack of the relaxing effect of NO in the VSMC, but rather a structural adaptation of the aortic wall. Indeed, NO is an important regulator of extracellular matrix protein crosslinking via S-nitrosylation of tissue transglutaminase (TG2). L-NAME treatment in WT mice is shown to correlate with an increase in TG activity and the associated increase in large artery stiffness can be prevented by genetically knocking out TG (45). More recently, it was shown in $eNOS^{-/-}$ mice that reduced S-nitrosylation of TG resulted in increased cross-linking activity and arterial stiffness, even in de-cellularized aortic segments. Moreover, arterial stiffness in $eNOS^{-/-}$ mice could be reversed by a 4 week treatment with the TG inhibitor cystamine (20).

Aortic ECs and VSMCs are subject to humoral, neurogenic and mechanical stimuli and altering VSMC tone will affect isobaric biomechanical properties of the aortic wall. Differences in VSMC and EC reactivity to circulating contractile agents such as catecholamines can affect the pulse-dampening capacity of the aorta (30). To estimate the contribution of eNOS expression on the maximal isobaric stiffness development, 2μM PE was added to the organ bath. The effect of PE on isobaric biomechanical parameters of WT and eNOS-tg aortic rings was remarkably small. We reported earlier that basal NO production in normal, healthy WT aorta will indeed protect against PE-induced increase in isobaric stiffness at normal pressure (30). The small effects of PE in the WT and eNOS-tg mice indicate that large amounts of basal NO are present in these tissues. On the contrary, the lack of NO production in the $eNOS^{-/-}$ aortic segments resulted in a ~5% reduction of isobaric diameter and a ~25% reduction in compliance at 80-120 mmHg. It can be hypothesized that, apart from the structural alterations in extracellular matrix and the resulting increase in passive stiffness, the lack of basal NO production in these mice will render them more susceptible to VSMC-contraction induced aortic stiffness *in vivo*, when circulating catecholamines are present.

To estimate the basal tone of VSMCs in KR solution, Ca^{2+} was removed from the extracellular fluid and the drop in isometric preload was assessed. This only affected $eNOS^{-/-}$ aortic rings, WT and eNOS-tg aortic segments showed no decrease of isometric preload. When basal NO production was blocked by adding L-NAME to the organ bath, the effect of 0Ca increased in eNOS-tg and WT aortic rings, but not in $eNOS^{-/-}$ mice. The fact that removal of basal NO in WT aortic segments results in a

317 higher baseline Ca^{2+} influx as compared to $eNOS^{-/-}$ mice, indicates that the VSMCs of the latter are
318 able to partially compensate for the increase in basal Ca^{2+}-influx by basal NO deficiency.

319 Adding PE in the absence of extracellular Ca^{2+} will result in a phasic contraction that reflects the
320 release of contractile Ca^{2+} from the sarcoplasmic reticulum. The amplitude of this contraction is larger
321 in $eNOS^{-/-}$ and eNOS-tg animals with interesting differences in the time constants of the relaxation
322 phase. The relaxation after the phasic contraction reflects removal of contractile Ca^{2+} from the cytosol
323 through the plasmalemmal Ca^{2+} ATPase and the Na/Ca exchanger (38), but is not due to re-uptake of
324 intracellular Ca^{2+} to the SR (27). The time constants of the relaxation phase indicate that, in eNOS-tg
325 animals, the relaxation phase was slow, while $eNOS^{-/-}$ mice are able to remove the Ca^{2+} very quickly
326 from the cytosol. Earlier, we showed that, in healthy mouse aortic segments, basal NO increases the
327 Ca^{2+}-content of intracellular stores of the VSMC, resulting in higher phasic contractions by PE in the
328 absence of extracellular Ca^{2+} and that blocking basal NO production results in slower relaxation (27).
329 Here, we show that the chronic absence of NO has an opposite effect on the relaxation. This might
330 reflect an adaptation mechanism by which the VSMCs are able to maintain intracellular Ca^{2+} levels
331 within an acceptable range. A possible explanation might be that in $eNOS^{-/-}$ mice, increased
332 plasmalemmal Ca^{2+} ATPase activity will remove more Ca^{2+} out of the cytosol at a faster rate, while in
333 eNOS-tg VSMCs, less Ca^{2+} is removed from the cytosol at a slower rate, to compensate for the
334 reduced Ca^{2+} influx caused by increased NO bioavailability. This is confirmed by the 0Ca experiment
335 showing that the baseline Ca^{2+} influx in $eNOS^{-/-}$ VSMC was less than half as compared the predicted
336 value based on the absence of NO alone (WT + L-NAME). It would be interesting to explore the Ca^{2+}
337 homeostasis in these mice further by investigating PMCA, Na/Ca exchanger and SERCA.

338 The tonic contraction resulting from Ca^{2+} re-addition in intracellular store-depleted VSMCs reflects
339 the influx of extracellular Ca^{2+} from the extracellular space into the cytosol, through both VGCC and
340 NSCCs (12). In normal conditions, the hyperpolarizing effect of NO will suppress Ca^{2+} influx.
341 Blocking NO production using L-NAME had almost no effect on the tonic contraction in $eNOS^{-/-}$
342 mice. Interestingly, there was no difference in the relative L-NAME effect between eNOS-tg and WT
343 mice. It has been reported that the eNOS activity in the aortic tissue of eNOS-tg mice is increased

~30-fold and NO production nearly doubled (15). This suggests that, despite the increase in eNOS activity and NO bioavailability, downstream pathways compensate for the reduced efficacy of NO. Indeed, NO desensitization is known to occur via S-nitrosylation of soluble guanylate cyclase in aortic VSMCs exposed to NO (46) and the opposite occurs in $eNOS^{-/-}$ mice (23). In addition, increased phosphodiesterase activity and, hence, increased enzymatic degradation of cGMP, is reported to occur in rat aortic VSMCs and human platelets quickly after exposure to NO (36).

We showed earlier that in healthy mouse aortic segments and in the presence of basal NO, the tonic contraction is mainly due to Ca^{2+} influx through VGCCs and only a minor part is caused by Ca^{2+} influx through non selective cation channels. This is confirmed in the present study; in WT and eNOS-tg mice, the tonic contraction is almost entirely through VGCCs. Upon addition of L-NAME, the NO-dependent suppression of NSCCs is lost, and this results in an increase of the NSCC-dependent contraction, while the VGCC contraction increases only slightly. Hence, L-NAME increases the relative contribution of NSCC vs VGCCs in WT and eNOS-tg mice, the opposite is true for $eNOS^{-/-}$ mice.

Overall, in this study we characterized the effects of acute and chronic absence of functional eNOS on the morphology, intrinsic biomechanics, basal VSMC tone, SR contractile Ca^{2+} content and the phasic as well as the tonic contraction properties of the isolated mouse aorta. We did not aim to fully investigate the mechanistic relationship between eNOS expression and vascular reactivity and biomechanics. The primary goal was to perform a vascular characterization that can be relevant when using these mouse models in vascular (biomechanical) research. When eNOS was present, the direction of the effects of pharmacological eNOS blockade using L-NAME were often – but not always – similar to the effects of chronic lack of eNOS expression in $eNOS^{-/-}$ mice. However, these effects were mostly of different magnitude, indicating the presence of compensatory mechanisms such as desensitization of NO targets in the VSMCs, as shown before (46). It might be interesting to further investigate which mechanisms, such as the prostanoid system, contribute to these phenomena in the future. It should however be noted that these animal models demonstrate different anomalies - as mentioned in the introduction - such as lower body weight, neurochemical and behavioral adaptations

for eNOS-/- mice, which might limit the use of these models to unravel the complex role of the NO signaling system in the large arteries. An additional limitation of our approach is that the organ bath does not match the physiological conditions. Perhaps due to the lack of low-molecular-weight thiols, which facilitate NO signal transduction in vivo (33), pharmacological addition or inhibition of NO release in the organ bath may differ from physiological activity of NO in the different animal models in vivo. Hence, one should be cautious translating the observations from the organ bath directly to the *in vivo* situation.

Our results suggest that altered Ca^{2+} handling in the VSMCs provide an additional compensatory mechanism by which the VSMCs maintain close to normal intracellular Ca^{2+} levels in mouse models with altered expression of eNOS. This appears to occur predominantly through altering the storage of contractile Ca^{2+} in the SR as well as through the removal of contractile Ca^{2+} from the cytosol. Further research is needed to identify the molecular pathways that specifically contribute to the observed differences in Ca^{2+}-handling in the aortic VSMCs of these mice.

Conflict of Interest

The authors declare that the research was conducted in the absence of any commercial or financial relationships that could be construed as a potential conflict of interest.

Author Contributions

AL, CVH, SDM and PF conceived and designed the experiments. Acquisition, analysis and interpretation of data were carried out by AL, CVH, SDM and PF in the laboratories of GDK and PF. The manuscript was drafted and critically revised by AL, SDM, CVH, GDK and PF. All authors have approved the final version of the manuscript and agree to be accountable for all aspects of the work. All persons designated as authors qualify for authorship, and all those who qualify for authorship are listed.

Funding

AL is supported by the Fund for Scientific Research (FWO) Flanders, grant number 11W3718N. SDM is supported by the GOA BOF 2017-2020 - project 33931

5. References

1. **Apter JT**, **Rabinowitz M**, **Cummings DH**. Correlation of Visco-elastic Properties of Large Arteries with Microscopic Structure. *Circ Res* 19: 104–121, 1966.

2. **Balligand J-L**, **Feron O**, **Dessy C**. eNOS Activation by Physical Forces: From Short-Term Regulation of Contraction to Chronic Remodeling of Cardiovascular Tissues. *Physiol Rev* 89: 481–534, 2009.

3. **Barra JG**, **Armentano RL**, **Levenson J**, **Fischer EI**, **Pichel RH**, **Simon A**. Assessment of smooth muscle contribution to descending thoracic aortic elastic mechanics in conscious dogs. *Circ Res* 73: 1040–50, 1993.

4. **Benetos A**, **Safar M**, **Rudnichi A**, **Smulyan H**, **Richard JL**, **Ducimetieère P**, **Guize L**. Pulse pressure: a predictor of long-term cardiovascular mortality in a French male population. *Hypertension* 30: 1410–5, 1997.

5. **Borlotti A**, **Khir AW**, **Rietzschel ER**, **De Buyzere ML**, **Vermeersch S**, **Segers P**. Noninvasive determination of local pulse wave velocity and wave intensity: changes with age and gender in the carotid and femoral arteries of healthy human. *J Appl Physiol* 113: 727–35, 2012.

6. **Brutsaert DL**, **Claes VA**. Onset of mechanical activation of mammalian heart muscle in calcium- and strontium-containing solutions. *Circ Res* 35: 345–57, 1974.

7. **Brutsaert DL**, **Claes VA**, **Sonnenblick EH**. Effects of abrupt load alterations on force-velocity-length and time relations during isotonic contractions of heart muscle: load clamping. *J Physiol* 216: 319–30, 1971.

8. **Demas GE**, **Kriegsfeld LJ**, **Blackshaw S**, **Huang P**, **Gammie SC**, **Nelson RJ**, **Snyder SH**. Elimination of aggressive behavior in male mice lacking endothelial nitric oxide synthase. *J Neurosci* 19: RC30, 1999.

9. **Dere E**, **De Souza Silva MA**, **Topic B**, **Fiorillo C**, **Li JS**, **Sadile AG**, **Frisch C**, **Huston JP**. Aged endothelial nitric oxide synthase knockout mice exhibit higher mortality concomitant with impaired open-field habituation and alterations in forebrain neurotransmitter levels. *Genes Brain Behav* 1: 204–13, 2002.

10. **Dinardo CL**, **Venturini G**, **Zhou EH**, **Watanabe IS**, **Campos LCG**, **Dariolli R**, **da Motta-Leal-Filho JM**, **Carvalho VM**, **Cardozo KHM**, **Krieger JE**, **Alencar AM**, **Pereira AC**. Variation of mechanical properties and quantitative proteomics of VSMC along the arterial tree. *Am J Physiol Heart Circ Physiol* 306: H505-16, 2014.

11. **Feng W**, **Gang L**, **Xin G**, **Han ZQ**, **Yu XW**, **You QJ**. Overexpression of eNOS decrease tissue factor (TF) level in CD34+ cells exhibit increased antithrombogenic property in small caliber vascular graft. *J. Cardiovasc. Surg. (Torino).* .

12. **Fransen P**, **Van Hove CECE**, **Leloup AJAJA**, **Martinet W**, **De Meyer GRYGRY**, **Lemmens K**, **Bult H**, **Schrijvers DMDM**. Dissecting out the complex Ca2+-mediated phenylephrine-induced contractions of mouse aortic segments. *PLoS One* 10: e0121634, 2015.

13. **Freedman JE**, **Sauter R**, **Battinelli EM**, **Ault K**, **Knowles C**, **Huang PL**, **Loscalzo J**. Deficient platelet-derived nitric oxide and enhanced hemostasis in mice lacking the NOSIII gene. *Circ Res* 84: 1416–21, 1999.

14. **Gyurko R**, **Kuhlencordt P**, **Fishman MC**, **Huang PL**. Modulation of mouse cardiac function in vivo by eNOS and ANP. *Am J Physiol Heart Circ Physiol* 278: H971-81,

2000.

15. **van Haperen R**, **Cheng C**, **Mees BME**, **van Deel E**, **de Waard M**, **van Damme LCA**, **van Gent T**, **van Aken T**, **Krams R**, **Duncker DJ**, **de Crom R**. Functional Expression of Endothelial Nitric Oxide Synthase Fused to Green Fluorescent Protein in Transgenic Mice. *Am J Pathol* 163: 1677–1686, 2003.

16. **Van Hove CE**, **Van der Donckt C**, **Herman AG**, **Bult H**, **Fransen P**. Vasodilator efficacy of nitric oxide depends on mechanisms of intracellular calcium mobilization in mouse aortic smooth muscle cells. *Br J Pharmacol* 158: 920–30, 2009.

17. **Huang PL**, **Huang Z**, **Mashimo H**, **Bloch KD**, **Moskowitz MA**, **Bevan JA**, **Fishman MC**. Hypertension in mice lacking the gene for endothelial nitric oxide synthase. *Nature* 377: 239–242, 1995.

18. **Jablonka-Shariff A**, **Olson LM**. The Role of Nitric Oxide in Oocyte Meiotic Maturation and Ovulation: Meiotic Abnormalities of Endothelial Nitric Oxide Synthase Knock-Out Mouse Oocytes [1]. *Endocrinology* 139: 2944–2954, 1998.

19. **Jadhav UM**, **Kadam NN**. Non-invasive assessment of arterial stiffness by pulse-wave velocity correlates with endothelial dysfunction. *Indian Heart J* 57: 226–32, 2005.

20. **Jung SM**, **Jandu S**, **Steppan J**, **Belkin A**, **An SS**, **Pak A**, **Choi EY**, **Nyhan D**, **Butlin M**, **Viegas K**, **Avolio A**, **Berkowitz DE**, **Santhanam L**. Increased tissue transglutaminase activity contributes to central vascular stiffness in eNOS knockout mice. *Am J Physiol Heart Circ Physiol* 305: H803-10, 2013.

21. **Kaess BM**, **Rong J**, **Larson MG**, **Hamburg NM**, **Vita JA**, **Levy D**, **Benjamin EJ**, **Vasan RS**, **Mitchell GF**. Aortic stiffness, blood pressure progression, and incident hypertension. *JAMA* 308: 875–81, 2012.

22. **Kinlay S**, **Creager MA**, **Fukumoto M**, **Hikita H**, **Fang JC**, **Selwyn AP**, **Ganz P**. Endothelium-Derived Nitric Oxide Regulates Arterial Elasticity in Human Arteries In Vivo. *Hypertension* 38: 1049–1053, 2001.

23. **Kojda G**, **Laursen JB**, **Ramasamy S**, **Kent JD**, **Kurz S**, **Burchfield J**, **Shesely EG**, **Harrison DG**. Protein expression, vascular reactivity and soluble guanylate cyclase activity in mice lacking the endothelial cell nitric oxide synthase: contributions of NOS isoforms to blood pressure and heart rate control. *Cardiovasc Res* 42: 206–213, 1999.

24. **van Langen J**, **Fransen P**, **Van Hove CE**, **Schrijvers DM**, **Martinet W**, **De Meyer GRY**, **Bult H**. Selective loss of basal but not receptor-stimulated relaxation by endothelial nitric oxide synthase after isolation of the mouse aorta. *Eur J Pharmacol* 696: 111–9, 2012.

25. **Lantelme P**. Heart Rate: An Important Confounder of Pulse Wave Velocity Assessment. *Hypertension* 39: 1083–1087, 2002.

26. **Lee TC**, **Zhao YD**, **Courtman DW**, **Stewart DJ**. Abnormal aortic valve development in mice lacking endothelial nitric oxide synthase. *Circulation* 101: 2345–8, 2000.

27. **Leloup AJ**, **Van Hove CE**, **De Meyer GRY**, **Schrijvers DM**, **Fransen P**. Basal activity of voltage-gated Ca(2+) channels controls the IP3-mediated contraction by α(1)-adrenoceptor stimulation of mouse aorta segments. *Eur J Pharmacol* 760: 163–71, 2015.

28. **Leloup AJA**, **Fransen P**, **Van Hove CE**, **Demolder M**, **De Keulenaer GW**, **Schrijvers DM**. Applanation Tonometry in Mice: A Novel Noninvasive Technique to Assess Pulse Wave Velocity and Arterial Stiffness. *Hypertension* 64: 195–200, 2014.

29. **Leloup AJA**, **Van Hove CE**, **Heykers A**, **Schrijvers DM**, **De Meyer GRY**, **Fransen**

P. Elastic and Muscular Arteries Differ in Structure, Basal NO Production and Voltage-Gated Ca2+-Channels. *Front Physiol* 6: 375, 2015.

30. **Leloup AJA**, **Van Hove CE**, **Kurdi A**, **De Moudt S**, **Martinet W**, **De Meyer GRY**, **Schrijvers DM**, **De Keulenaer GW**, **Fransen P**. A novel set-up for the ex vivo analysis of mechanical properties of mouse aortic segments stretched at physiological pressure and frequency. *J Physiol* 594: 6105–6115, 2016.

31. **Leloup AJA**, **Van Hove CE**, **De Moudt S**, **De Meyer GRY**, **De Keulenaer GW**, **Fransen P**. Vascular smooth muscle cell contraction and relaxation in the isolated aorta: a critical regulator of large artery compliance. *Physiol Rep* 7: e13934, 2019.

32. **Leloup AJA**, **De Moudt S**, **Van Hove CE**, **Dugaucquier L**, **Vermeulen Z**, **Segers VFM**, **De Keulenaer GW**, **Fransen P**. Short-term angiotensin II treatment affects large artery biomechanics and function in the absence of small artery alterations in mice. *Front Physiol* 9, 2018.

33. **Loscalzo J**, The identification of nitric oxide as endothelium-derived relaxing factor. *Circ Res* 113:100–103, 2013.

34. **McEniery CM**, **Qasem A**, **Schmitt M**, **Avolio AP**, **Cockcroft JR**, **Wilkinson IB**. Endothelin-1 regulates arterial pulse wave velocity in vivo. *J Am Coll Cardiol* 42: 1975–1981, 2003.

35. **Mitchell GF**, **Moyé LA**, **Braunwald E**, **Rouleau JL**, **Bernstein V**, **Geltman EM**, **Flaker GC**, **Pfeffer MA**. Sphygmomanometrically determined pulse pressure is a powerful independent predictor of recurrent events after myocardial infarction in patients with impaired left ventricular function. SAVE investigators. Survival and Ventricular Enlargement. *Circulation* 96: 4254–60, 1997.

511 36. **Mullershausen F**, **Russwurm M**, **Thompson WJ**, **Liu L**, **Koesling D**, **Friebe A**.
512 Rapid nitric oxide-induced desensitization of the cGMP response is caused by
513 increased activity of phosphodiesterase type 5 paralleled by phosphorylation of the
514 enzyme. *J Cell Biol* 155: 271–8, 2001.

515 37. **Najjar SS**, **Scuteri A**, **Shetty V**, **Wright JG**, **Muller DC**, **Fleg JL**, **Spurgeon HP**,
516 **Ferrucci L**, **Lakatta EG**. Pulse wave velocity is an independent predictor of the
517 longitudinal increase in systolic blood pressure and of incident hypertension in the
518 Baltimore Longitudinal Study of Aging. *J Am Coll Cardiol* 51: 1377–83, 2008.

519 38. **Nazer MA**, **van Breemen C**. Functional linkage of Na(+)-Ca2+ exchange and
520 sarcoplasmic reticulum Ca2+ release mediates Ca2+ cycling in vascular smooth
521 muscle. *Cell Calcium* 24: 275–83, 1998.

522 39. **Palanisamy AP**, **Cheng G**, **Sutter AG**, **Liu J**, **Lewin DN**, **Chao J**, **Chavin K**.
523 Adenovirus-Mediated eNOS Expression Augments Liver Injury after
524 Ischemia/Reperfusion in Mice. *PLoS One* 9: e93304, 2014.

525 40. **Peng X**, **Haldar S**, **Deshpande S**, **Irani K**, **Kass DA**. Wall stiffness suppresses
526 Akt/eNOS and cytoprotection in pulse-perfused endothelium. *Hypertension* 41: 378–
527 81, 2003.

528 41. **Razny U**, **Kiec-Wilk B**, **Polus A**, **Wator L**, **Dyduch G**, **Partyka L**, **Bodzioch M**,
529 **Tomaszewska R**, **Wybranska I**. The adipose tissue gene expression in mice with
530 different nitric oxide availability. *J Physiol Pharmacol* 61: 607–18, 2010.

531 42. **Ruitenbeek AG**, **van der Cammen TJM**, **van den Meiracker AH**, **Mattace-Raso**
532 **FUS**. Age and blood pressure levels modify the functional properties of central but not
533 peripheral arteries. *Angiology* 59: 290–5, 2008.

534 43. **Safar ME**, **Nilsson PM**, **Blacher J**, **Mimran A**. Pulse pressure, arterial stiffness, and
535 end-organ damage. *Curr Hypertens Rep* 14: 339–44, 2012.

536 44. **Sansbury BE**, **Cummins TD**, **Tang Y**, **Hellmann J**, **Holden CR**, **Harbeson MA**,
537 **Chen Y**, **Patel RP**, **Spite M**, **Bhatnagar A**, **Hill BG**. Overexpression of Endothelial
538 Nitric Oxide Synthase Prevents Diet-Induced Obesity and Regulates Adipocyte
539 Phenotype. *Circ Res* 111: 1176–1189, 2012.

540 45. **Santhanam L**, **Tuday EC**, **Webb AK**, **Dowzicky P**, **Kim JH**, **Oh YJ**, **Sikka G**, **Kuo**
541 **M**, **Halushka MK**, **Macgregor AM**, **Dunn J**, **Gutbrod S**, **Yin D**, **Shoukas A**, **Nyhan**
542 **D**, **Flavahan NA**, **Belkin AM**, **Berkowitz DE**. Decreased S-nitrosylation of tissue
543 transglutaminase contributes to age-related increases in vascular stiffness. *Circ Res*
544 107: 117–25, 2010.

545 46. **Sayed N**, **Baskaran P**, **Ma X**, **van den Akker F**, **Beuve A**. Desensitization of soluble
546 guanylyl cyclase, the NO receptor, by S-nitrosylation. *Proc Natl Acad Sci U S A* 104:
547 12312–7, 2007.

548 47. **Schmitt M**, **Avolio A**, **Qasem A**, **McEniery CM**, **Butlin M**, **Wilkinson IB**,
549 **Cockcroft JR**. Basal NO Locally Modulates Human Iliac Artery Function In Vivo.
550 *Hypertension* 46: 227–231, 2005.

551 48. **Shesely EG**, **Maeda N**, **Kim HS**, **Desai KM**, **Krege JH**, **Laubach VE**, **Sherman PA**,
552 **Sessa WC**, **Smithies O**. Elevated blood pressures in mice lacking endothelial nitric
553 oxide synthase. *Proc Natl Acad Sci U S A* 93: 13176–81, 1996.

554 49. **Soucy KG**, **Ryoo S**, **Benjo A**, **Lim HK**, **Gupta G**, **Sohi JS**, **Elser J**, **Aon M a**, **Nyhan**
555 **D**, **Shoukas AA**, **Berkowitz DE**. Impaired shear stress-induced nitric oxide production
556 through decreased NOS phosphorylation contributes to age-related vascular stiffness. *J*

Appl Physiol 101: 1751–9, 2006.

50. **Tsuprykov O**, **Chaykovska L**, **Kretschmer A**, **Stasch J-P**, **Pfab T**, **Krause-Relle K**, **Reichetzeder C**, **Kalk P**, **Adamski J**, **Hocher B**. Endothelin-1 Overexpression Improves Renal Function in eNOS Knockout Mice. *Cell Physiol Biochem* 37: 1474–1490, 2015.

51. **Vignon-Zellweger N**, **Relle K**, **Kienlen E**, **Alter M**, **Seider P**, **Sharkovska J**, **Heiden S**, **Kalk P**, **Schwab K**, **Albrecht-Küpper B**, **Theuring F**, **Stasch J-P**, **Hocher B**. Endothelin-1 overexpression restores diastolic function in eNOS knockout mice. *J Hypertens* 29: 961–970, 2011.

52. **Van Vliet BN**, **Chafe LL**, **Montani J-P**. Characteristics of 24 h Telemetered Blood Pressure in eNOS-Knockout and C57Bl/6J Control Mice. *J Physiol* 549: 313–325, 2003.

53. **Weisbrod RM**, **Shiang T**, **Al Sayah L**, **Fry JL**, **Bajpai S**, **Reinhart-King CA**, **Lob HE**, **Santhanam L**, **Mitchell G**, **Cohen RA**, **Seta F**. Arterial Stiffening Precedes Systolic Hypertension in Diet-Induced Obesity. *Hypertension* 62: 1105–10, 2013.

54. **Wilkinson IB**, **Qasem A**, **McEniery CM**, **Webb DJ**, **Avolio AP**, **Cockcroft JR**. Nitric oxide regulates local arterial distensibility in vivo. *Circulation* 105: 213–7, 2002.

55. **Zhang Y**, **Agnoletti D**, **Protogerou AD**, **Topouchian J**, **Wang J-G**, **Xu Y**, **Blacher J**, **Safar ME**. Characteristics of pulse wave velocity in elastic and muscular arteries: a mismatch beyond age. *J Hypertens* 31: 554–9; discussion 559, 2013.

Figure legends.

Figure 1: Diastolic diameter (A), compliance (B) and Ep (C) were determined while segments were stretched at physiological frequency (10 Hz) between preloads corresponding to transmural pressures of 80 and 120 mmHg. One-way ANOVA with Bonferroni post-hoc test for multiple comparison: *, **, ***: P< 0.05, 0.01, 0.001 vs WT, NS: not significant, P>0.05. Lines and error bars represent mean and 95% confidence intervals, respectively.

Figure 2: *D*iastolic diameter (A), compliance (B) and Ep (C) with the VSMCs maximally relaxed using 2 µM DEANO differ between groups, while the relative effects (vs. baseline in Krebs-Ringer) on diastolic diameter (D_0), compliance (E) and Ep (F) are similar. One-way ANOVA with Bonferroni post-hoc test for multiple comparison: *, **, ***: P<0.05, 0.01, 0.001 vs WT, NS: not significant, P>0.05. Lines and error bars represent means and 95% confidence intervals, respectively.

Figure 3: Maximal development of active stiffness. Absolute values in contracted conditions (A-C) and the relative effects of maximal contraction using 2 µM PE (D-F) on diastolic diameter (1st column, A, D), compliance (2nd column, B, E) and Ep (3th column, C, F). One-way ANOVA with Bonferroni post-hoc test for multiple comparison: *, **, ***: P<0.05, 0.01, 0.001 vs WT, NS: not significant, P>0.05. Lines and error bars represent mean and 95% confidence intervals, respectively.

Figure 4: Hematoxylin and eosin (first row), orcein (second row) and Sirius red (third row) staining of aortic segments of WT (first column), eNOS$^{-/-}$ (second column) and eNOS-tg (third column) mice. Magnification is 10 X and the scale bar represents 200 µm.

Figure 5. Wall structure parameters (internal circumference (A), wall thickness (B), wall surface (C), number of VSMCs per µm^2 wall surface (D), relative amount of elastin (E) and collagen (F), as based on microscopic staining with H&E, Sirius red and orcein (Figure 5). One-way ANOVA with

605 Bonferroni post-hoc test for multiple comparison: *, **, *** P<0.05, 0.01, 0.001 vs. WT. Lines and
606 error bars represent mean and 95% confidence intervals, respectively.
607
608 Figure 6. Basal tone of aortic segments of WT, eNOS$^{-/-}$ and eNOS-tg mice upon removal of external
609 Ca^{2+} in the absence (A) and presence (B) of 300 μM L-NAME. Two-way ANOVA with repeated
610 measures (eNOS active-blocked) and Bonferroni post-hoc test for multiple comparison: *: P<0.05:
611 eNOS$^{-/-}$ versus WT (A), eNOS-tg versus eNOS$^{-/-}$ (B); #, ###: P<0.05, 0.001: eNOS inhibited versus
612 eNOS active. Lines and error bars represent mean and 95% confidence intervals, respectively.
613
614 Figure 7. α_1-Adrenoceptor stimulation of aortic segments of WT, eNOS$^{-/-}$ and eNOS-tg mice
615 (n=5/group) in the absence of extracellular Ca^{2+} and in the absence (A) and presence of 300 μM L-
616 NAME (B). Phasic contractions were fitted with a double exponential function revealing amplitude
617 (C) and time constant (E) of the contractile phase and amplitude (D) and time constant (F) of the
618 relaxing phase. Symbols (A-B) or lines (C-F) and error bars represent mean and 95% confidence
619 intervals, respectively. Two-way ANOVA with repeated measures (eNOS active-blocked) and
620 Bonferroni post-hoc test for multiple comparison: *, **, ***: P<0.05, 0.01, 0.001 versus WT; #, ##:
621 P<0.05, 0.01 + L-NAME versus – L-NAME. Symbols (A-B) or lines (C-F) and error bars represent
622 means and 95 % confidence intervals, respectively.
623
624 Figure 8. Tonic contractions by PE, evoked by adding external Ca^{2+} to the 0Ca solution containing 1
625 μM PE, in the absence (A) and presence (B) of 300 μM L-NAME to segments of WT (white), eNOS$^{-/-}$
626 (red) and eNOS-tg mice (n=5/group). The effect of PE at 600 s is shown in C, whereas the relative
627 contraction in the absence of L-NAME with respect to the presence of L-NAME is shown in D.
628 Kruskal-Wallis with Dunn's post-hoc test for multiple comparison (D) or repeated measures two-way
629 ANOVA (eNOS active-blocked) and Bonferroni post-hoc test for multiple comparison (A-C): *, **,
630 ***: P<0.05, 0.01 and 0.001 eNOS$^{-/-}$ or eNOS-tg versus WT; ##:P<0.01 + L-NAME versus –L-
631 NAME. Symbols (A-B) or lines (C) and error bars represent means (A-C) or median (D) and 95%
632 confidence intervals, respectively.

Figure 9*:* Absolute (A and B) and relative (C and D) effects of 35 μM diltiazem (A and C) and 50 μM 2-APB (B and D) on the tonic contractions elicited by 1 μM PE (Figure 8). Two-way ANOVA with repeated measures (eNOS active-blocked) and Bonferroni post-hoc test for multiple comparison: *, **, ***: P<0.5, 0.01, 0.001 $eNOS^{-/-}$ or eNOS-tg versus WT; #, ##, ###: P<0.05, 0.01, 0.001 +L-NAME versus –L-NAME. Lines and error bars represent mean and 95% confidence intervals, respectively.

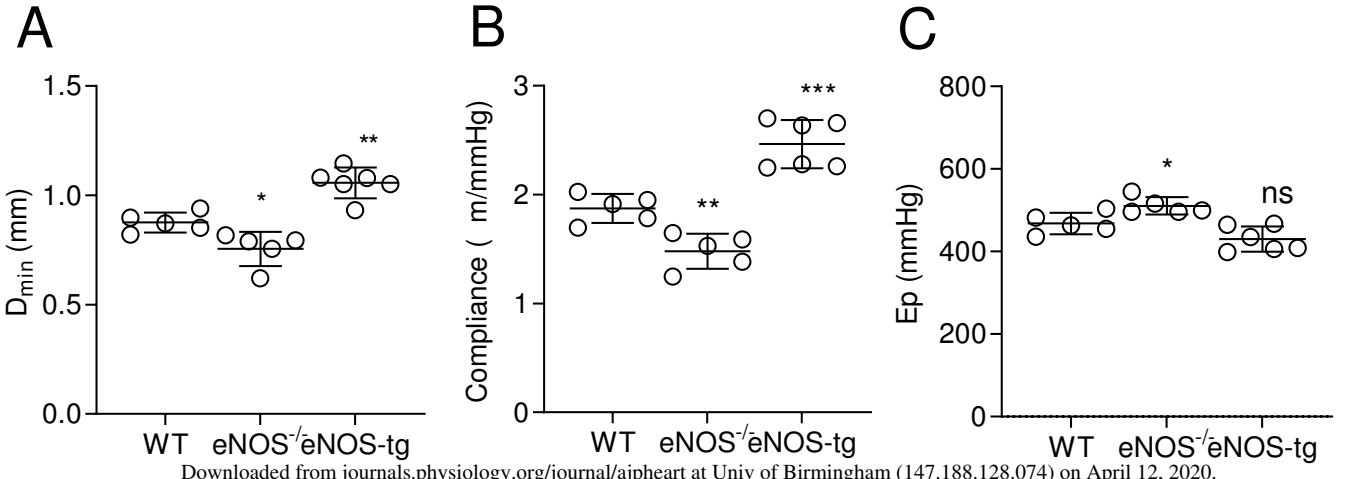

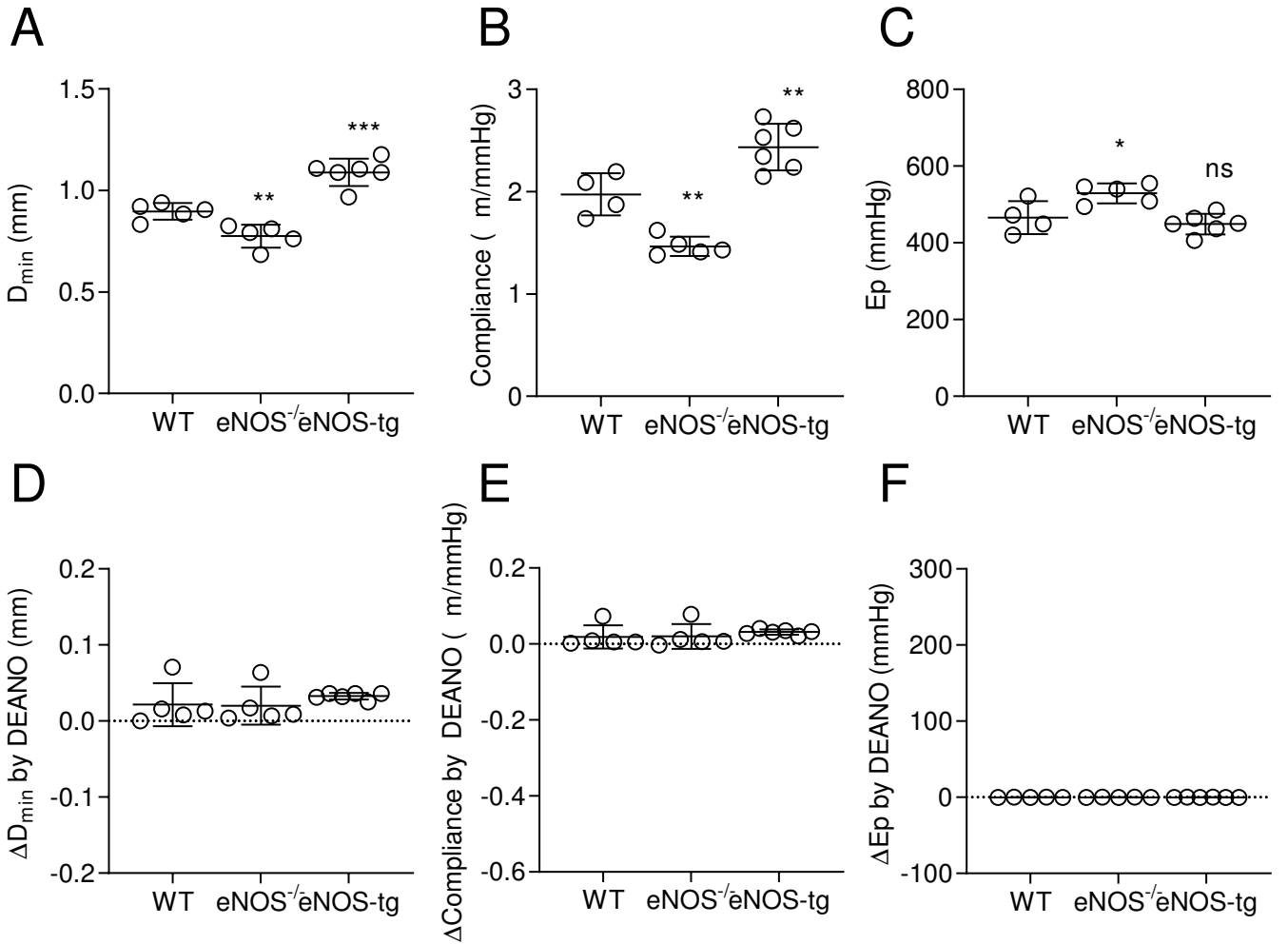

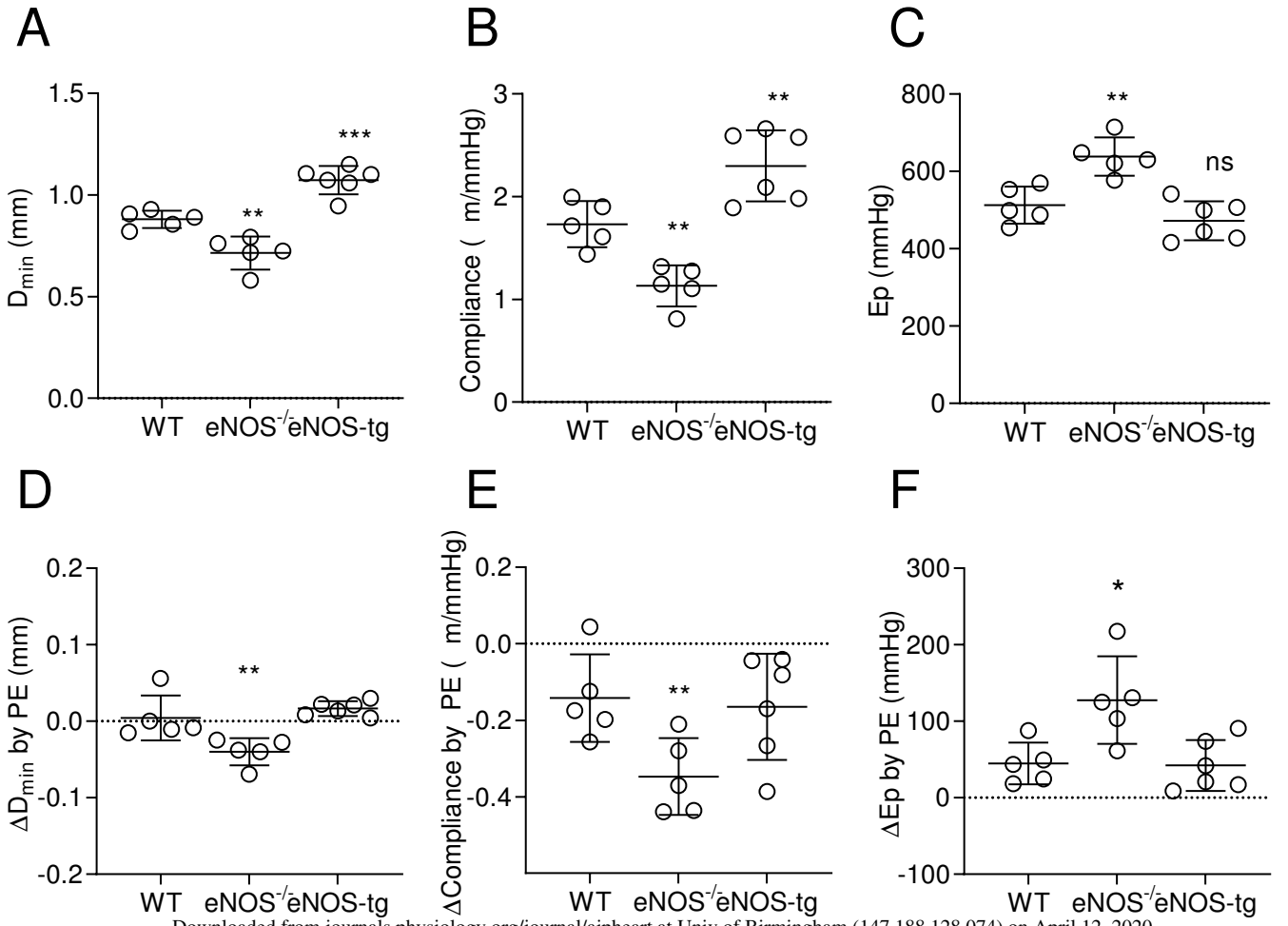

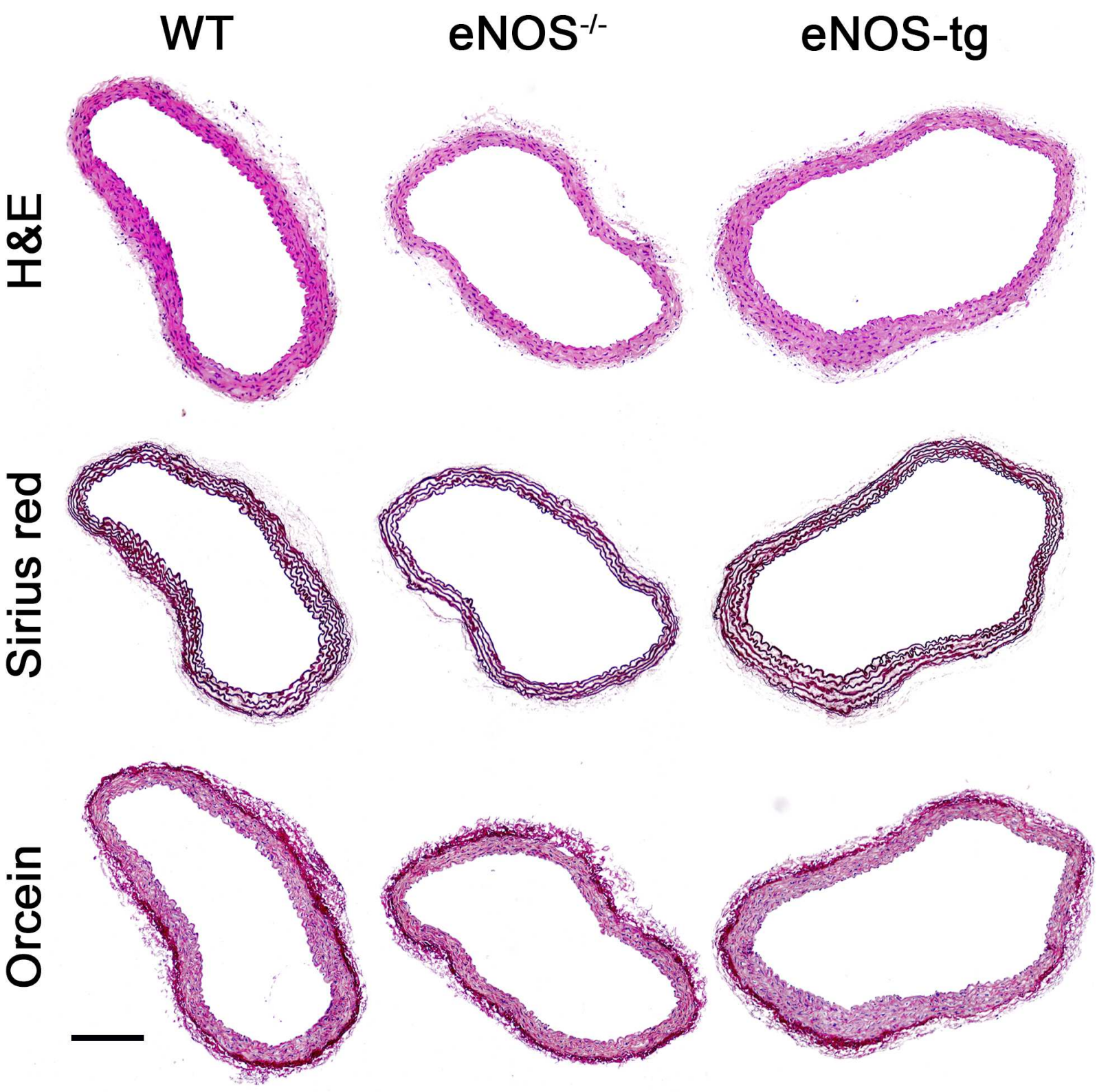

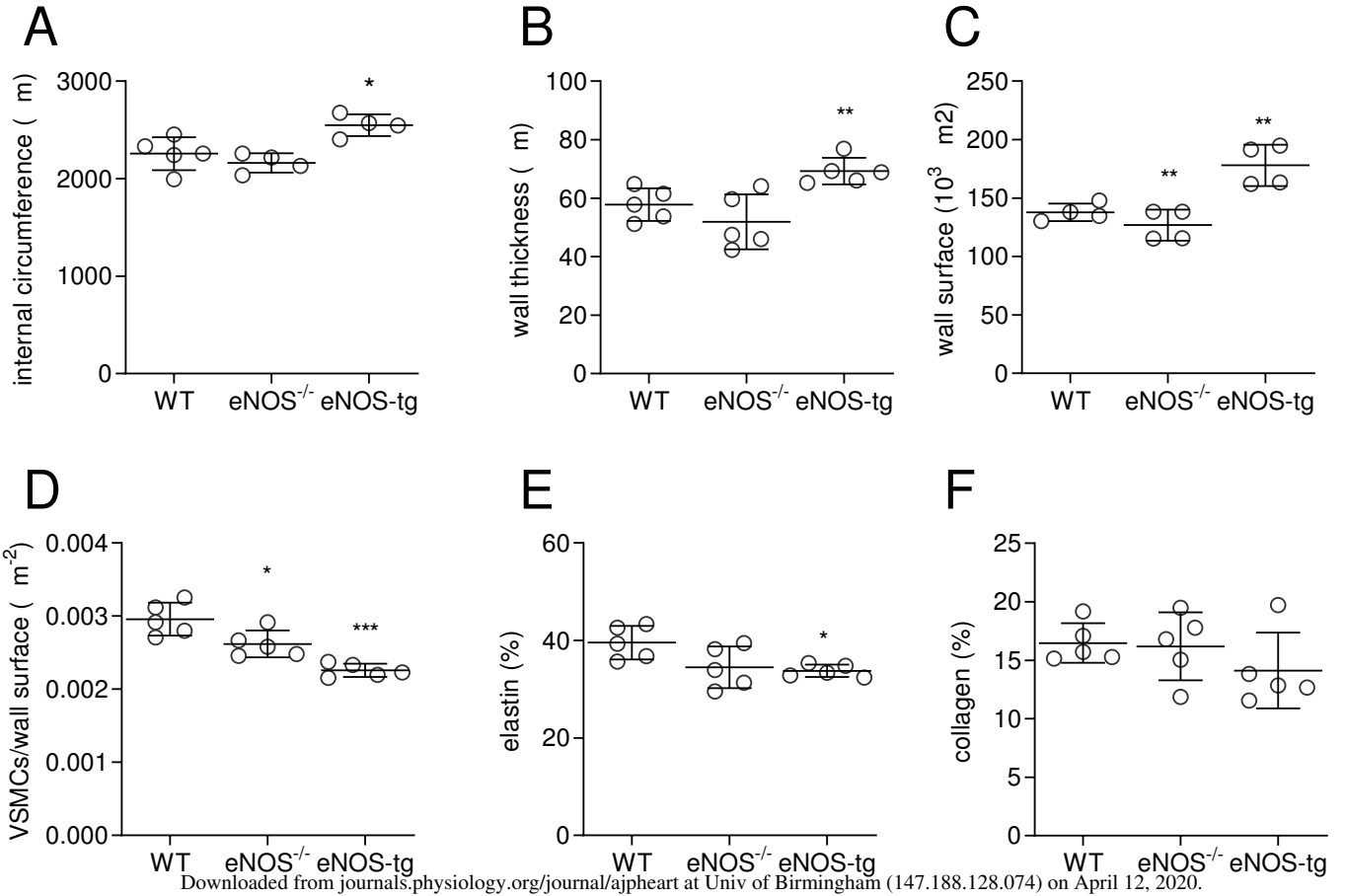

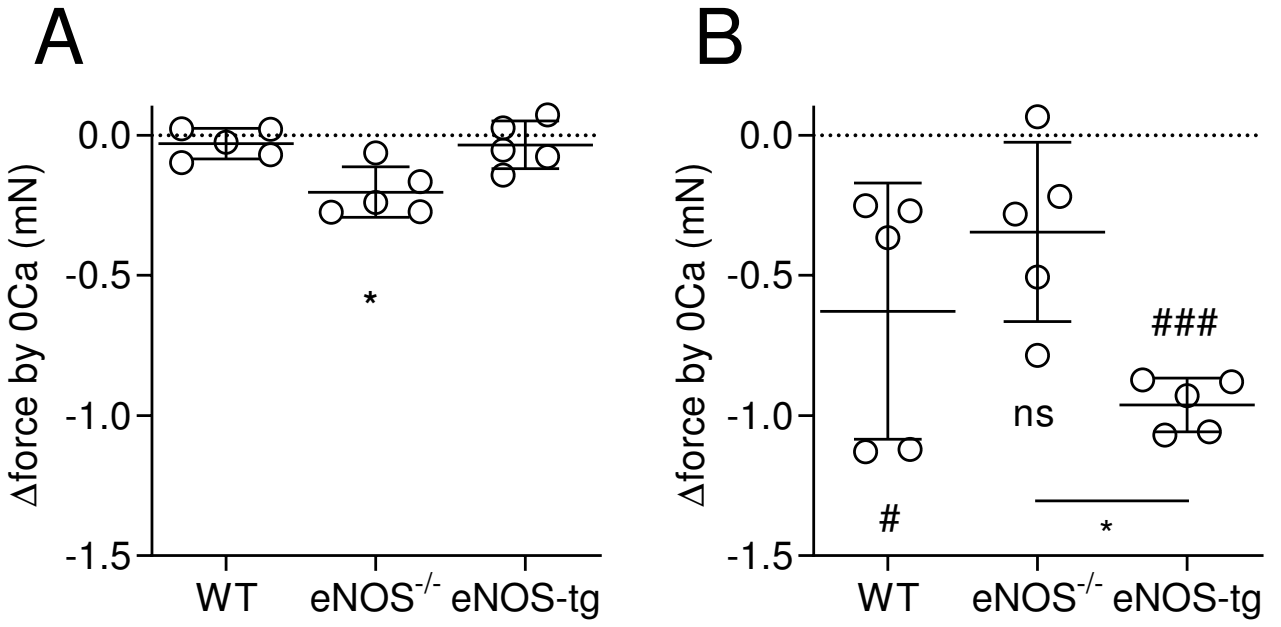

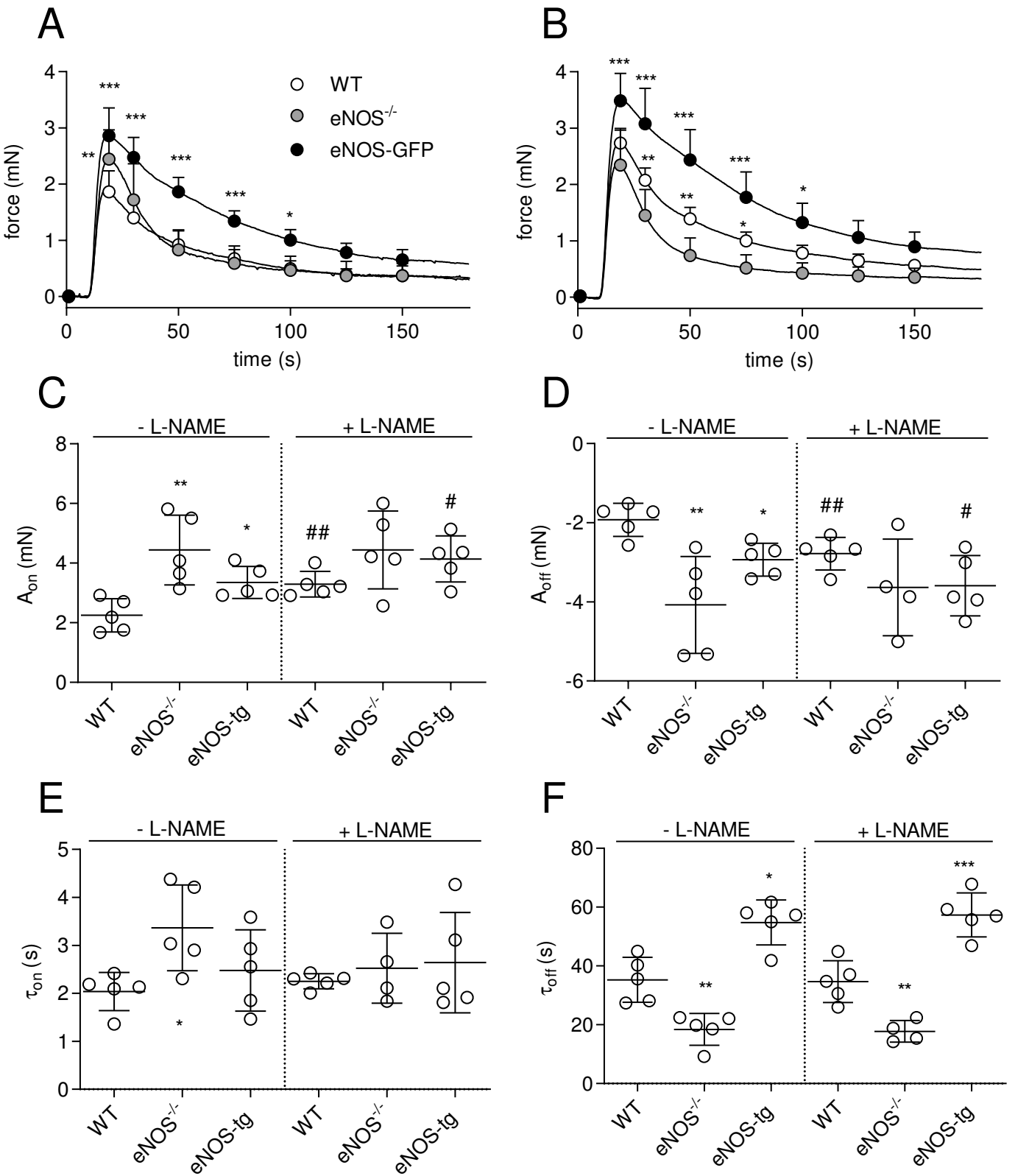

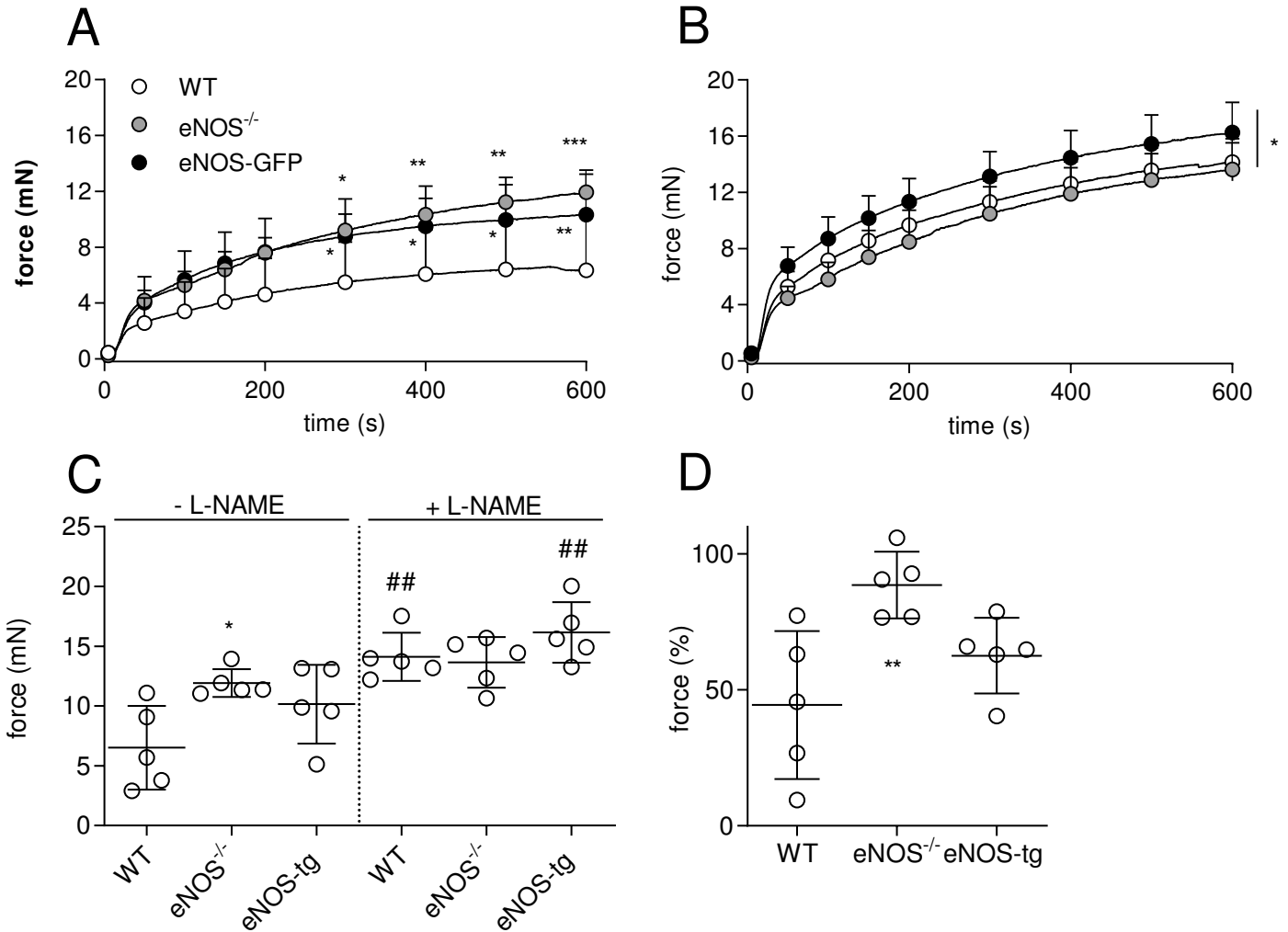

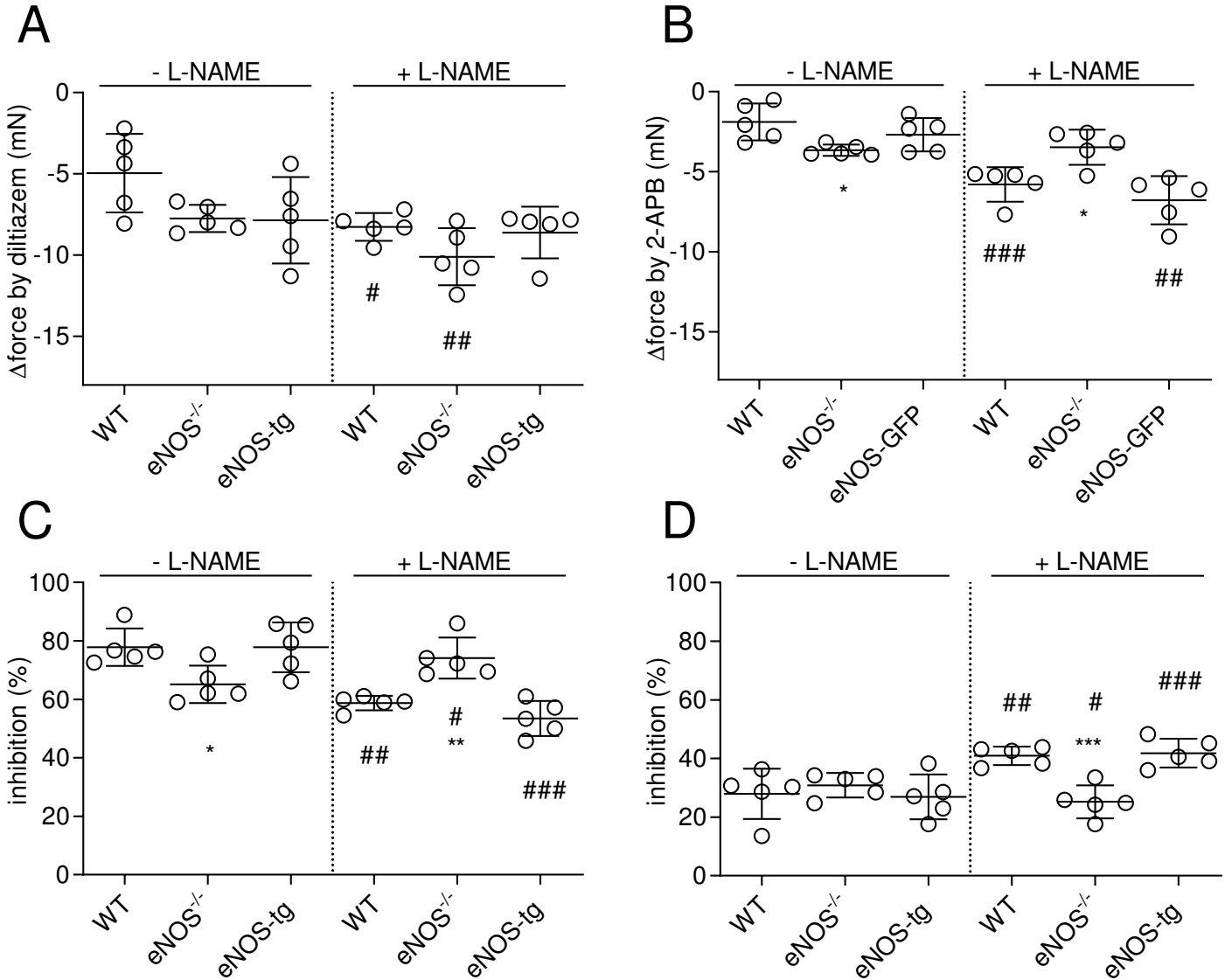

	Morphology	Passive biomechanics	Reactivity
eNOS$^{-/-}$	Diameter ↓ VSMC content ↓ Elastin ≈ Collagen ≈	Compliance ↓ Ep ↑	Basal tone ↑ SR Ca2+ content ↑ Ca2+ extrusion ↓ PE contractility ↑
eNOS-tg	Diameter ↑ VSMC content ↓ ↓ Elastin ↓ Collagen ≈	Compliance ↑ Ep ≈	Basal tone ≈ SR Ca2+ content ↑ ↑ Ca2+ extrusion ↑ ↑ PE contractility ≈

Table 1: Main qualitative changes in the isolated aorta of both mouse models as compared to WT mice aortic segments with respect to morphology, passive biomechanical parameters as well as the active changes in vascular reactivity.